INTERNATIONAL JOURNAL OF CLIMATOLOGY
Int. J. Climatol. **22**: 1571–1592 (2002)
Published online in Wiley InterScience (www.interscience.wiley.com). DOI: 10.1002/joc.846

A DROUGHT CLIMATOLOGY FOR EUROPE

BENJAMIN LLOYD-HUGHES[a,*] and MARK A. SAUNDERS[a,b]
[a] *Department of Space and Climate Physics, University College London, Holmbury St Mary, Dorking, Surrey RH5 6NT, UK*
[b] *Benfield Greig Hazard Research Centre, University College London, Gower Street, London WC1E 6BT, UK*

Received 5 February 2002
Revised 17 June 2002
Accepted 17 June 2002

ABSTRACT

We present a high spatial resolution, multi-temporal climatology for the incidence of 20th century European drought. The climatology provides, for a given location or region, the time series of drought strength, the number, the mean duration, and the maximum duration of droughts of a given intensity, and the trend in drought incidence. The drought climatology is based on monthly standardized precipitation indices (SPIs) calculated on a 0.5° grid over the European region 35–70 °N and 35 °E–10 °W at time scales of 3, 6, 9, 12, 18, and 24 months for the period 1901–99. The standardized property facilitates the quantitative comparison of drought incidence at different locations and over different time scales. The standardization procedure (probability transformation) has been tested rigorously assuming normal, log–normal, and gamma statistics for precipitation. Near equivalence is demonstrated between the Palmer drought severity index (PDSI) and SPIs on time scales of 9 to 12 months. The mean number and duration by grid cell of extreme European drought events (SPI $\leqslant -2$) on a time scale of 12 months is 6 ± 2 months and 27 ± 8 months respectively. The mean maximum drought duration is 48 ± 17 months. Trends in SPI and PDSI values indicate that the proportion of Europe experiencing extreme and/or moderate drought conditions has changed insignificantly during the 20th century. We hope the climatology will provide a useful resource for assessing both the regional vulnerability to drought and the seasonal predictability of the phenomenon. Copyright © 2002 Royal Meteorological Society.

KEY WORDS: climatology; drought; Europe; PDSI; precipitation; SPI

1. INTRODUCTION

Drought is a recurrent feature of the European climate that is not restricted to the Mediterranean region: it can occur in high and low rainfall areas and in any season (European Environment Agency, 2001). Large areas of Europe have been affected by drought during the 20th century. Recent severe and prolonged droughts have highlighted Europe's vulnerability to this natural hazard and alerted the public, governments, and operational agencies to the many socio-economic problems accompanying water shortage and to the need for drought mitigation measures.

A consistent framework for the description of drought is essential for any study of the phenomenon. Unfortunately, there is no generally accepted classification scheme (Wilhite and Glantz, 1985). It is possible to define drought in terms of meteorological, hydrological, agricultural, and socio-economic conditions. This has resulted in a large number of drought index parameters being found in the literature.

Precipitation is the primary factor controlling the formation and persistence of drought conditions, but evapotranspiration is also an important variable. Historical difficulties in quantifying evapotranspiration rates suggest that a general classification scheme is best limited to a simple measure of rainfall. Indeed, indices based solely on precipitation data perform well when compared with more complex hydrological indices (Oladipio, 1985). This paper describes the calculation of a new drought climatology for Europe based upon

* Correspondence to: Benjamin Lloyd-Hughes, Department of Space and Climate Physics, University College London, Holmbury St Mary, Dorking, Surrey RH5 6NT, UK; e-mail: blh@mssl.ucl.ac.uk

a relatively new meteorological index, the standardized precipitation index (SPI) (McKee *et al*., 1993). The SPI is compared against the traditional Palmer drought severity index (PDSI) (Palmer, 1965), which is a soil moisture algorithm that includes terms for water storage and evapotranspiration.

Although there have been many regional European drought studies (e.g. Gibb *et al*., 1978; Marsh and Lees, 1985; Phillips and McGregor, 1998; Bussay *et al*., 1999; Estrela *et al*., 2000; Lana *et al*., 2001), few authors have examined pan-European drought incidence. Indeed, only Briffa *et al*.(1994) have attempted to document drought across Europe as a whole. Their study employed the PDSI and focused on summer moisture variability for the period 1892–1991 at a spatial resolution of 5°. Summer droughts are the most important in terms of human perception, but water shortages during the other seasons also have significant socio-economic impacts (European Environment Agency, 2001).

Recent European initiatives in studying drought include the Assessment of the Regional Impact of Droughts in Europe (ARIDE) project (Demuth and Stahl, 2001) and the Water Resources: Influence of Climate Change in Europe (WRINCLE) project (Kilsby, 2001). Whilst ARIDE has a hydrological focus, meteorological drought is considered in the development of a regional classification scheme for streamflow drought. Large-scale droughts are analysed using standardized monthly precipitation anomalies and regionalized using a clustering technique. The principal objective of WRINCLE is to provide detailed future projections for hydrological climate across Europe. As part of this project, drought statistics are compiled using both the PDSI and a scheme based on accumulated monthly precipitation deficits.

The PDSI is known to be problematic (Alley, 1984; Oladipio, 1985), but is seen as useful for comparing with the SPI because of its widespread use in the United States of America, and through its use in the studies of European drought by Briffa *et al*.(1994) and by the WRINCLE project. Section 2 provides a description of the PDSI followed by a detailed discussion and derivation of the SPI. We apply the latter methodology to compute the SPI for the period 1901–99 at a latitude/longitude resolution of 0.5° by 0.5° over the European region 35°–70 °N and 35 °E–10 °W. The SPI is calculated for a range of time scales (3, 6, 9, 12, 18, and 24 months) to provide a choice of index appropriate for different meteorological, agricultural and hydrological applications. Section 3 presents climatological results on drought incidence for individual locations and for Europe as a whole; namely the number, mean duration, and maximum duration of droughts of a given intensity, and the trend in drought incidence. A discussion of these results is presented in Section 4, and conclusions are drawn in Section 5.

2. METHODOLOGY

2.1. Data

Gridded precipitation and temperature data are taken from the monthly 0.5° set compiled by the Climatic Research Unit (CRU) at the University of East Anglia (New *et al*., 2000). These data cover the period 1901–98. Data for 1999 are obtained from the University of Delaware monthly terrestrial air temperature and precipitation grids (Version 1.02). Soil water-holding capacities, required for the PDSI calculations, are those estimated by Reynolds *et al*.(1999) from the Food and Agriculture Organization digital soil map of the world CD-ROM (FAO, 1996). These are regridded from 5′ resolution to 0.5° using bilinear interpolation.

2.2. Drought index calculations

2.2.1. PDSI. The PDSI is based upon a set of empirical relationships derived by Palmer (1965) to express regional moisture supply standardized in relation to local climatological norms. It has been used widely in the United States of America since its introduction in 1965. There have been many applications of the PDSI in the literature (e.g. Karl, 1983; Soulé, 1992; Nigam *et al*., 1999) and several critiques (e.g. Alley, 1984; Oladipio, 1985).

The index is a sum of the current moisture anomaly and a fraction of the previous index value. The moisture anomaly is defined as

$$d = P - \hat{P} \tag{1}$$

where P is the total monthly precipitation, and $\hat{P}$ is the precipitation value 'climatologically appropriate for existing conditions' (Palmer 1965). $\hat{P}$ represents the water balance equation defined as

$$\hat{P} = \overline{\mathrm{ET}} + \overline{R} + \overline{\mathrm{RO}} - \overline{L} \tag{2}$$

where $\overline{\mathrm{ET}}$ is the evapotranspiration, $\overline{R}$ is the soil water recharge, $\overline{\mathrm{RO}}$ is the run off, and $\overline{L}$ is the water loss from the soil. The overbars signify that these are average values for the given month taken over some calibration period. $\hat{P}$ is a hydrological factor and needs be parameterized locally.

The Palmer moisture anomaly index (Z index) is then defined as

$$Z = Kd \tag{3}$$

and the PDSI for month i is defined as

$$\mathrm{PDSI}_i = 0.897\mathrm{PDSI}_{i-1} + Z_i/3 \tag{4}$$

K acts as a climate weighting factor and is applied to yield indices with comparable local significance in space and time. The resultant PDSI values are broken down into 11 categories, ranging from extremely dry to extremely wet. These are listed in Table I. As implied in the above description, the PDSI is usually calculated over a monthly period. However, there is nothing to prevent calculations across other time periods, e.g. weekly or bi-monthly.

The principal advantage of the PDSI is its 'standardized' nature, which facilitates the quantitative comparison of drought incidence at different locations and different times. However, the empirical relationships used to define the index (in particular K, the climate weighting factor) were determined by observations taken from only nine US climate stations. This limited number brings the general applicability of the scaling process into question Alley, (1984).

A clear and detailed description of the steps required to calculate the PDSI can be found in Alley (1984) and need not be repeated here. We employ all the available data to calibrate the climate weighting factors K. Temperature normals, needed to estimate the potential evapotranspiration, are taken for the period 1961–90.

2.2.2. SPI.

2.2.2.1. Background: A deficit of precipitation impacts on soil moisture, stream flow, reservoir storage, and ground water level, etc. on different time scales. McKee *et al*. (1993) developed the SPI to quantify

Table I. Drought classification by PDSI value

PDSI value	Classification
4.00 or more	Extremely wet
3.00 to 3.99	Very wet
2.00 to 2.99	Moderately wet
1.00 to 1.99	Slightly wet
0.50 to 0.99	Incipient wet spell
0.49 to −0.49	Near normal
−0.50 to −0.99	Incipient dry spell
−1.00 to −1.99	Mild drought
−2.00 to −2.99	Moderate drought
−3.00 to −3.99	Severe drought
−4 or less	Extreme drought

precipitation deficits on multiple time scales. The SPI is simply the transformation of the precipitation time series into a standardized normal distribution (z-distribution).

Bussay *et al*. (1998) and Szalai and Szinell (2000) assessed the utility of the SPI for describing drought in Hungary. They concluded that the SPI was suitable for quantifying most types of drought event. Stream flow was described best by SPIs with time scales of 2–6 months. Strong relationships to ground water level were found at time scales of 5–24 months. Agricultural drought (proxied by soil moisture content) was replicated best by the SPI on a scale of 2–3 months. Lana *et al*. (2001) recently used the SPI to investigate patterns of rainfall over Catalonia, Spain.

Hayes *et al*. (1999) discuss the advantages and disadvantages of using the SPI to characterize drought severity. The SPI has three main advantages. The first and primary advantage is simplicity. The SPI is based solely on rainfall and requires only the computation of two parameters, compared with the 68 computational terms needed to describe the PDSI. By avoiding dependence on soil moisture conditions, the SPI can be used effectively in both summer and winter. The SPI is also not affected adversely by topography. The SPI's second advantage is its variable time scale, which allows it to describe drought conditions important for a range of meteorological, agricultural, and hydrological applications. This temporal versatility is also helpful for the analysis of drought dynamics, especially the determination of onset and cessation, which have always been difficult to track with other indices. The third advantage comes from its standardization, which ensures that the frequency of extreme events at any location and on any time scale are consistent. The SPI has three potential disadvantages, the first being the assumption that a suitable theoretical probability distribution can be found to model the raw precipitation data prior to standardization. An associated problem is the quantity and reliability of the data used to fit the distribution. McKee *et al*. (1993) recommend using at least 30 years of high-quality data. A second limitation of the SPI arises from the standardized nature of the index itself; namely that extreme droughts (or any other drought threshold) measured by the SPI, when considered over a long time period, will occur with the same frequency at all locations. Thus, the SPI is not capable of identifying regions that may be more 'drought prone' than others. A third problem may arise when applying the SPI at short time scales (1, 2, or 3 months) to regions of low seasonal precipitation. In these cases, misleadingly large positive or negative SPI values may result.

The SPI is computed by fitting a probability density function to the frequency distribution of precipitation summed over the time scale of interest. This is performed separately for each month (or whatever the temporal basis is of the raw precipitation time series) and for each location in space. Each probability density function is then transformed into the standardized normal distribution. Thus, the SPI is said to be normalized in location and time scale, sharing the benefits of standardization described for the PDSI. Once standardized, the strength of the anomaly is classified as set out in Table II. This table also contains the corresponding probabilities of occurrence of each severity, these arising naturally from the normal probability density function. Thus, at a given location for an individual month, moderate droughts (SPI $\leqslant -1$) have an occurrence probability of 15.9%, whereas extreme droughts (SPI $\leqslant -2$) have an event probability of 2.3%. Extreme values in the SPI will, by definition, occur with the same frequency at all locations.

Table II. Drought classification by SPI value and corresponding event probabilities

SPI value	Category	Probability %
2.00 or more	Extremely wet	2.3
1.50 to 1.99	Severely wet	4.4
1.00 to 1.49	Moderately wet	9.2
0 to 0.99	Mildly wet	34.1
0 to −0.99	Mild drought	34.1
−1.00 to −1.49	Moderate drought	9.2
−1.50 to −1.99	Severe drought	4.4
−2 or less	Extreme drought	2.3

2.2.2.2. Calculation: The monthly precipitation time series are modelled using different statistical distributions. The first is the gamma distribution, whose probability density function is defined as

$$g(x) = \frac{1}{\beta^{\alpha}\Gamma(\alpha)} x^{\alpha-1} \mathrm{e}^{-x/\beta} \qquad \text{for} \quad x > 0 \tag{5}$$

where $\alpha > 0$ is a shape parameter, $\beta > 0$ is a scale parameter, and $x > 0$ is the amount of precipitation. $\Gamma(\alpha)$ is the gamma function, which is defined as

$$\Gamma(\alpha) = \lim_{n\to\infty} \prod_{v=0}^{n-1} \frac{n! n^{y-1}}{y+v} \equiv \int_0^{\infty} y^{\alpha-1} \mathrm{e}^{-y}\, \mathrm{d}y \tag{6}$$

Fitting the distribution to the data requires α and β to be estimated. Edwards & McKee (1997) suggest estimating these parameters using the approximation of Thom (1958) for maximum likelihood as follows:

$$\hat{\alpha} = \frac{1}{4A}\left(1 + \sqrt{1 + \frac{4A}{3}}\right) \tag{7}$$

$$\hat{\beta} = \frac{\overline{x}}{\hat{\alpha}} \tag{8}$$

where, for n observations

$$A = \ln(\overline{x}) - \frac{\sum \ln(x)}{n} \tag{9}$$

This approach can be refined using an iterative procedure suggested by Wilks (1995):

$$\begin{aligned} \begin{bmatrix} \alpha* \\ \beta* \end{bmatrix} &= \begin{bmatrix} \hat{\alpha} \\ \hat{\beta} \end{bmatrix} - \begin{bmatrix} \frac{\partial^2 L}{\partial \hat{\alpha}^2} & \frac{\partial^2 L}{\partial \hat{\alpha}\partial \hat{\beta}} \\ \frac{\partial^2 L}{\partial \hat{\alpha}\partial \hat{\beta}} & \frac{\partial^2 L}{\partial \hat{\beta}^2} \end{bmatrix}^{-1} \begin{bmatrix} \frac{\partial L}{\partial \hat{\alpha}} \\ \frac{\partial L}{\partial \hat{\beta}} \end{bmatrix} \\ &= \begin{bmatrix} \hat{\alpha} \\ \hat{\beta} \end{bmatrix} - \begin{bmatrix} -n\Gamma''(\hat{\alpha}) & \frac{-n}{\hat{\beta}} \\ \frac{-n}{\hat{\beta}} & \frac{n\hat{\alpha}}{\hat{\beta}^2} - \frac{2\Sigma x}{\hat{\beta}^3} \end{bmatrix}^{-1} \begin{bmatrix} \Sigma \ln(x) - n\ln(\hat{\beta}) - n\Gamma'(\hat{\alpha}) \\ \frac{\Sigma x}{\hat{\beta}^2} - \frac{n\hat{\alpha}}{\hat{\beta}} \end{bmatrix} \end{aligned} \tag{10}$$

where $\alpha*$ and $\beta*$ are generally better estimates of α and β than $\hat{\alpha}$ and $\hat{\beta}$. The process is repeated until the algorithm converges. If no convergence is detected Thom's estimates for α and β are used. As in the PDSI calculations, all available data are used to fit these parameters.

Integrating the probability density function with respect to x and inserting the estimates of α and β yields an expression for the cumulative probability $G(x)$ of an observed amount of precipitation occurring for a given month and time scale:

$$G(x) = \int_0^x g(x)\, \mathrm{d}x = \frac{1}{\hat{\beta}^{\hat{\alpha}}\Gamma(\hat{\alpha})} \int_0^x x^{\hat{\alpha}} \mathrm{e}^{-x/\hat{\beta}}\, \mathrm{d}x \tag{11}$$

Substituting t for $x/\hat{\beta}$ reduces Equation (11) to

$$G(x) = \frac{1}{\Gamma(\hat{\alpha})} \int_0^x t^{\hat{\alpha}-1} \mathrm{e}^{-1}\, \mathrm{d}t \tag{12}$$

which is the incomplete gamma function. Values of the incomplete gamma function are computed using an algorithm taken from Press *et al*. (1986). Since the gamma distribution is undefined for $x = 0$, and $q = P(x = 0) > 0$ where $P(x = 0)$ is the probability of zero precipitation, the cumulative probability becomes

$$H(x) = q + (1 - q)G(x) \tag{13}$$

The cumulative probability distribution is then transformed into the standard normal distribution to yield the SPI. This process is illustrated in Figure 1. The first panel shows the empirical cumulative probability distribution for a 3 month average December–January–February (DJF) of precipitation over the south east of England for the period 1901–99. Over-plotted is the theoretical cumulative probability distribution of the fitted gamma distribution. The second panel displays a graph of standard normal cumulative probability. To convert a given precipitation level, say 77 mm, to its corresponding SPI value, first locate 77 mm on the abscissa of the left-hand panel, draw a perpendicular, and locate the point of intersection with the theoretical distribution. Then project this point horizontally (maintaining equal cumulative probability) until it intersects with the graph of standard normal cumulative probability. The intersection between a line drawn vertically downward from this point and the abscissa determines the SPI value (1.1 in this example).

The above approach, whilst simple, is not practical for computing the SPI for large numbers of data points. Following Edwards and McKee (1997), we employ the approximate conversion provided by Abramowitz and Stegun (1965) as an alternative:

$$Z = \mathrm{SPI} = -\left(t - \frac{c_0 + c_1 t + c_2 t^2}{1 + d_1 t + d_2 t^2 + d_3 t^3}\right) \quad \text{for} \quad 0 < H(x) \leq 0.5 \tag{14}$$

$$Z = \mathrm{SPI} = +\left(t - \frac{c_0 + c_1 t + c_2 t^2}{1 + d_1 t + d_2 t^2 + d_3 t^3}\right) \quad \text{for} \quad 0.5 < H(x) < 1 \tag{15}$$

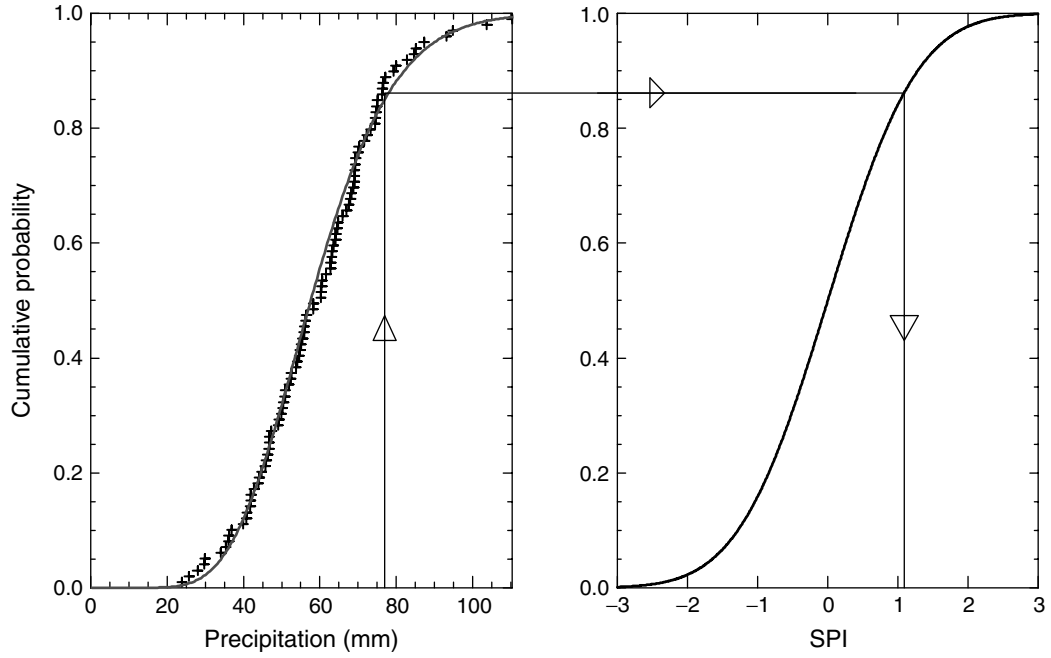

Figure 1. Example of an equiprobability transformation from a fitted gamma distribution to the standard normal distribution. Data are for the 3 month (DJF) average precipitation over the southeast of England. (After Edwards and McKee (1997))

where

$$t = \sqrt{\ln\left[\frac{1}{(H(x))^2}\right]} \qquad \text{for} \quad 0 < H(x) \leq 0.5 \tag{16}$$

$$t = \sqrt{\ln\left[\frac{1}{(1 - H(x))^2}\right]} \quad \text{for} \quad 0.5 < H(x) < 1 \tag{17}$$

and

$$\begin{aligned} &c_0 = 2.515\,517 \quad c_1 = 0.802\,853 \quad c_2 = 0.010\,328 \\ &d_1 = 1.432\,788 \quad d_2 = 0.189\,269 \quad d_3 = 0.001\,308 \end{aligned} \tag{18}$$

2.2.2.3. Other distributions: It is possible that precipitation in some regions or at particular time scales may be modelled better by a distribution other than the gamma. For instance, Lana *et al*. (2001) found the Poisson-gamma distribution to be useful for modelling precipitation in Catalonia. Another possibility is the log–normal distribution. In common with the gamma distribution, the log–normal distribution is positively skewed and non-negative. It has the advantage of simplicity since it is just a logarithmic transformation of the data (Wilks, 1995), i.e. $Y = \ln(x)$ (for $x > 0$), with the assumption that the resulting transformed data are described by a Gaussian distribution. On fitting the log–normal distribution with the sample mean and variance of the transformed data, $\hat{\mu_y}$ and $\hat{\sigma}_y^2$, the SPI becomes simply

$$\text{SPI} = Z = \frac{\ln(x) - \hat{\mu_y}}{\hat{\sigma_y}} \tag{19}$$

The central limit theorem suggests that, as we move to extended time periods in excess of 6 months, the resultant time averaging will tend to shift the observed probability distributions towards normal. Because the gamma distribution tends towards the normal as the shape parameter α tends to infinity, it would be computationally more efficient to standardize the data directly from a fitted normal distribution where possible, i.e. to take

$$\text{SPI} = Z = \frac{(x - \hat{\mu})}{\hat{\sigma}} \tag{20}$$

where again $\hat{\mu}$ and $\hat{\sigma}$ are the sample estimates of the population mean and standard deviation respectively.

To assess how well a given distribution describes the data, it is possible to compare the empirical cumulative probability distribution with the corresponding theoretical cumulative probability distribution. This is formalized using the Kolmogorov–Smirnov (K–S) test statistic

$$D_n = \max_x |F_n(x) - F(x)| \tag{21}$$

where $F_n(x)$ is the empirical cumulative probability, estimated as $F_n(x_{(i)}) = i/n$ for the ith smallest data value. $F(x)$ is the theoretical cumulative probability distribution evaluated at x. Under the null hypothesis that the data are drawn from the theoretical distribution, D_n is compared with tabulated values appropriate to the sample size and the assumed distribution. If D_n exceeds the critical value, the null hypothesis is rejected at the given level of significance. The test becomes more complicated when the distribution parameters are estimated from the *same* sample population as that used to compute the empirical probability distribution. A narrowing of the confidence interval results (as tabulated by Wilks (1995). In these circumstances the K–S test is known as the Lilliefors test (Wilks, 1995).

3. RESULTS

3.1. Suitability of the gamma distribution

We computed the multi-temporal SPI values by modelling the precipitation data with different statistical distributions. We tested the assumption that the gamma distribution would provide the best representation of the data by computing monthly K–S statistics for each grid cell at each time scale using gamma, log–normal, and normal distributions. Figures 2 and 3 illustrate the pass/fail status of the Lilliefors test at the 5% significance level, at time scales of 3 months and 12 months respectively, for (a) the normal distribution and (b) the gamma distribution. The gamma distribution is shown to be a good fit for all months at both time scales (<15% of grid cells fail the test). The fit to the normal distribution improves as the time scale of interest is extended, thereby indicating that aggregates of precipitation can be taken to be distributed approximately normally for time scales in excess of 12 months. Figure 2(a) illustrates the poor performance of the normal distribution at the 3 month time scale (∼25% failure). The fit is worst for regions south of 45 °N. These are arid regions where the distribution of precipitation is more skewed. This is confirmed by the poorest fits occurring in late summer to early autumn, where monthly rainfall totals are at their lowest. Similar results were obtained for other time scales. In general, the log–normal distribution fitted less well than the gamma distribution, yielding results similar to the normal distribution.

We note that none of the distributions tested could adequately model precipitation over eastern Turkey or across northwest Spain. This was true for all months and at every time scale. Figure 4(a) shows a cumulative probability distribution representative of the Turkish region. The smooth curve is the fitted gamma distribution. The fitted distribution fails to capture the sharp rise seen in the central section of the empirical distribution. The steep gradient indicates the most probable rainfall lies within a narrow band of totals. This is illustrated in Figure 4(b), which is a histogram of the same data. Over-plotted are the theoretical distributions corresponding to the normal, log–normal, and gamma distributions. They each capture the tails of the data, but none represents the narrow peak in the centre of the histogram. The same picture is seen in the data for northwest Spain (not shown).

To test the validity of the equiprobability transform, K–S statistics were computed for each of the SPI indices under the null hypothesis that the transformed data are distributed normally with zero mean and unit variance. Not unsurprisingly, failure, that is rejection of the null hypothesis at the 5% significance level, was confined to northwest Spain and eastern Turkey. Elsewhere, the transformation was found to be successful and the corresponding SPI values were taken as valid. Only data passing the above tests were retained for further analysis. This led to the rejection of between 6 and 15% of the data, dependent on month and time scale. However, at least 3000 grid cells Europe-wide were always retained.

3.2. Validation of the index calculations

The PDSI calculations were validated by comparing maps with the summer PDSI values published by Briffa *et al*. (1994). The two computations were found to be in excellent agreement. A similar approach was used to validate the SPI calculations. Maps of SPI3 derived from the CRU 0.5° data for the USA were compared with those published by Edwards and McKee (1997) computed from station data. The different maps were in complete agreement. These comparisons validate our SPI calculation, and show that index values computed from gridded data are representative of those obtainable from station data.

3.3. European drought climatology

3.3.1. Temporal intercomparison of indices. Area averages of SPI3, 6, 9, 12, 18, 24, and PDSI have been calculated for the entire European region. Each grid cell was weighted according to its area. Cross-correlations between the different indices are listed in Table III. The off-diagonal elements reveal a large degree of correlation between the indices. The PDSI is strongly correlated with the SPI at all time scales, with a peak of $r = 0.73$ at 9–12 months. This agrees with results published by Bussay *et al*. (1998) for the Hungarian region. SPI3 explains over 50% of the variance in SPI6, and over 30% of the variance in SPI9.

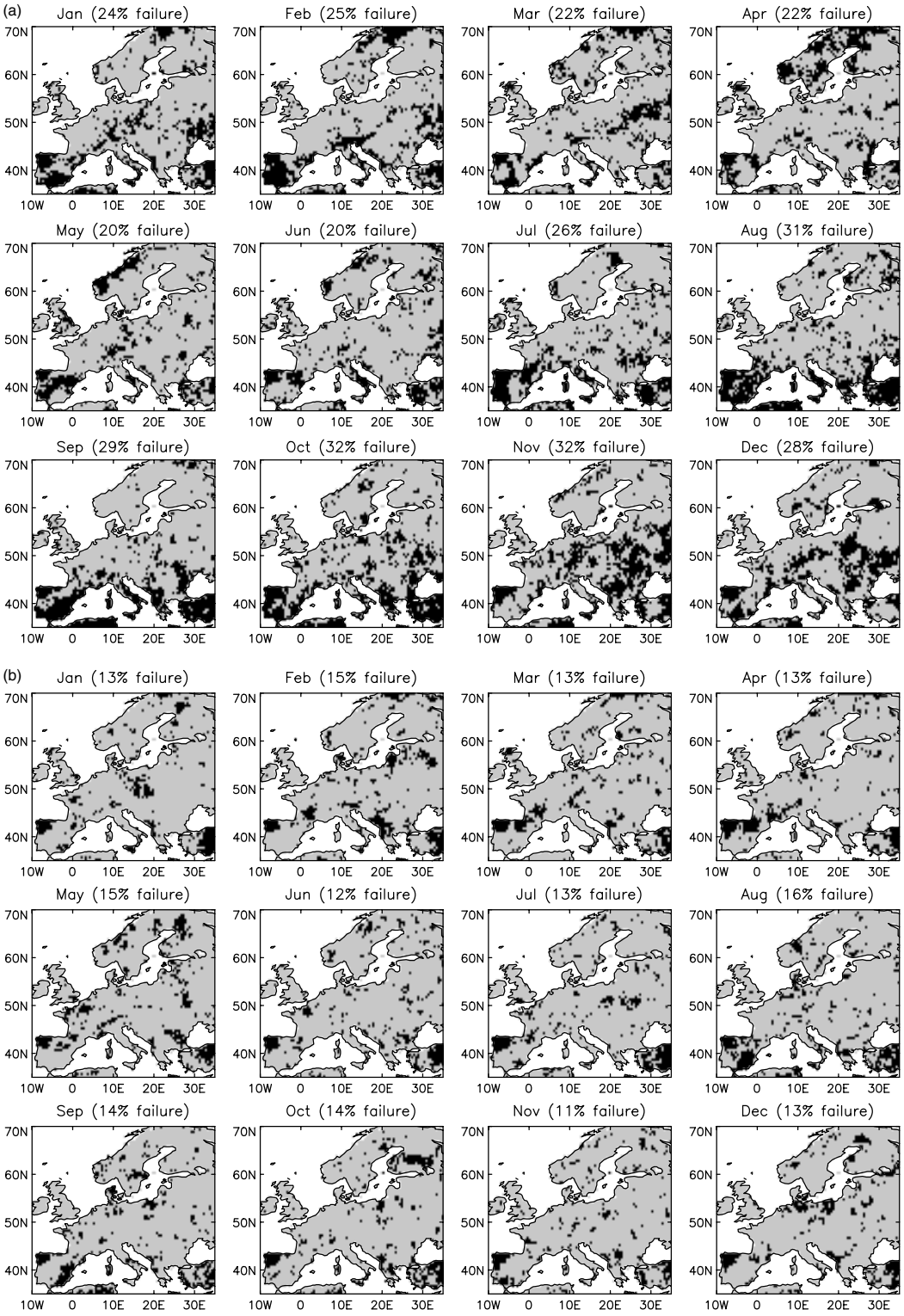

Figure 2. Lilliefors test results for SPI3 on monthly data 1901–99 using (a) normal and (b) gamma distributions. Black shading indicates rejection of the null hypothesis (that the distribution describes the data) at the 5% significance level. The proportion of grid cells failing the test is quoted at the top of each monthly panel

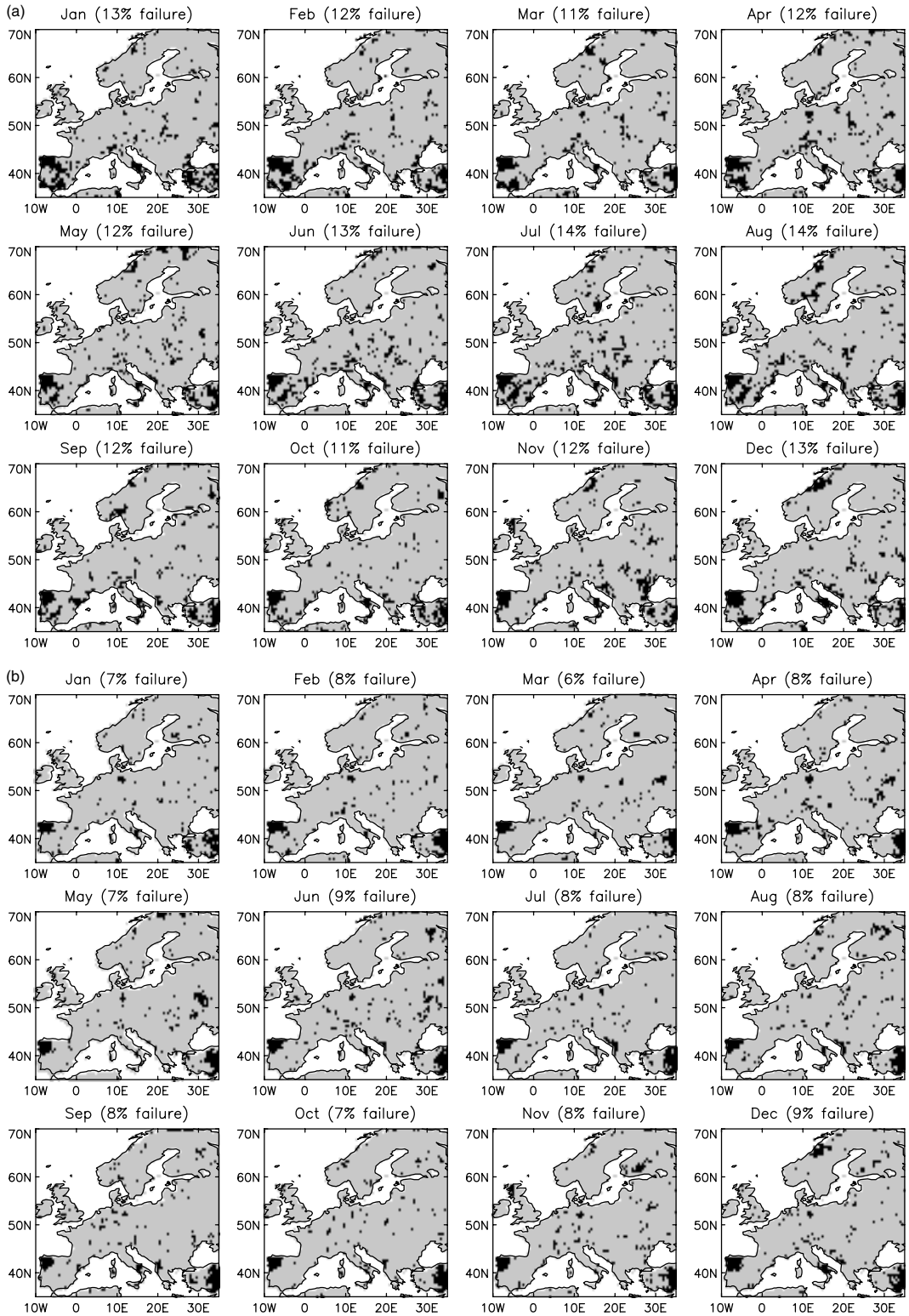

Figure 3. As for Figure 2, but for SPI12

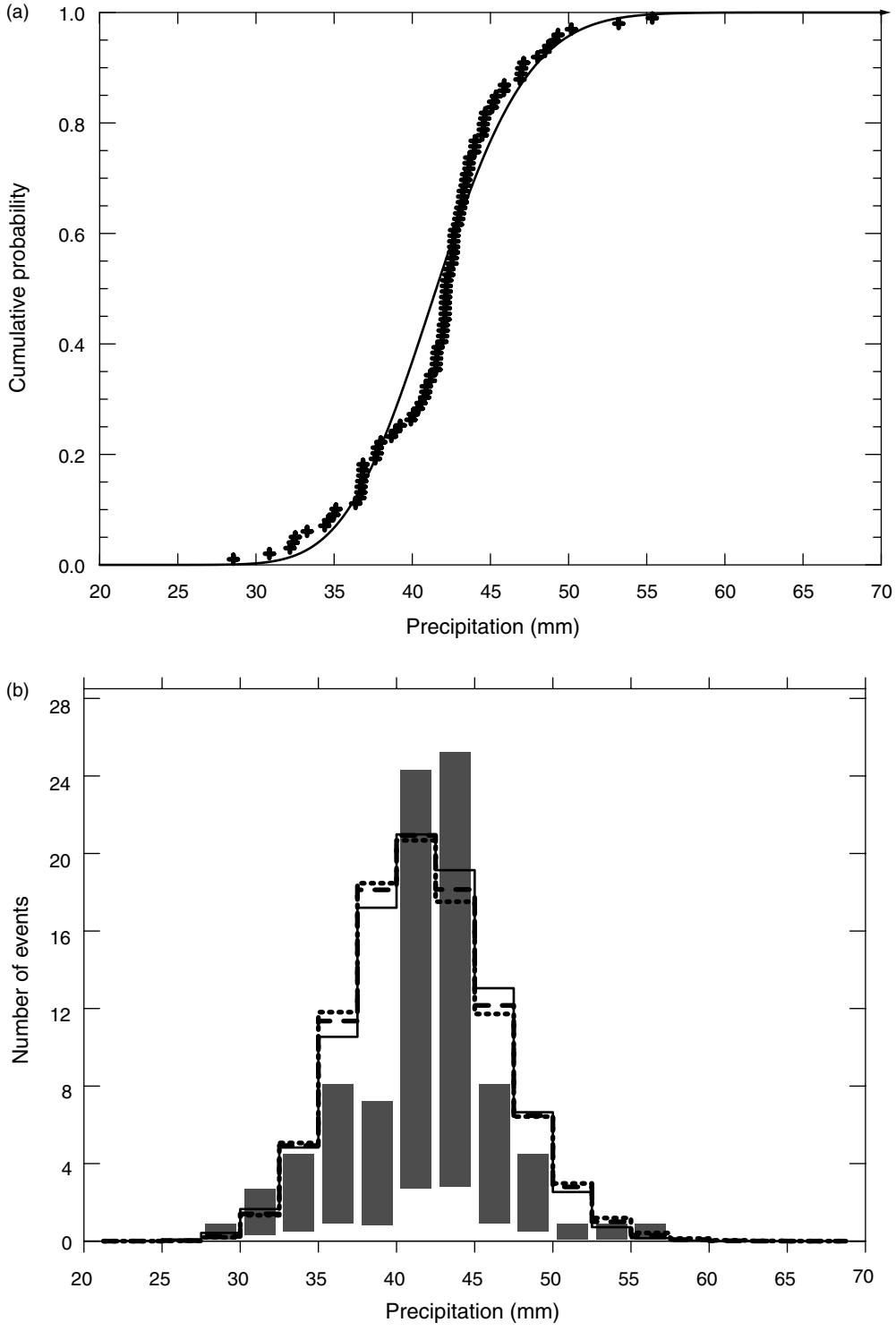

Figure 4. (a) Cumulative frequency distribution for July SPI12 over eastern Turkey. The smooth curve is the estimated gamma distribution. (b) Histogram of the same data. The shaded bars indicate the raw data. Over-plotted are theoretical distributions fitted to the data: normal (solid), log–normal (dotted), and gamma (dashed)

Table III. Cross-correlation between SPI3–24 and PDSI for European area average 1901–99. Each grid cell value is weighted according to area prior to computation of the average

SPI_n	3	6	9	12	18	24	PDSI
3	1	0.72	0.61	0.54	0.41	0.36	0.60
6		1	0.84	0.75	0.59	0.52	0.71
9			1	0.89	0.74	0.63	0.73
12				1	0.85	0.73	0.73
18					1	0.89	0.63
24						1	0.54
PDSI							1

Similarly, SPI12 explains over 70% of the variance in SPI18, and over 50% of the variance in both SPI24 and the PDSI.

The correlation between the SPI values at different temporal scales is further illustrated by the drought severity time series in Figure 5. The data are from a single grid cell centred on (0.75 °W, 53.75 °N) corresponding to South Dalton, North Yorkshire, UK. This is the same site used by Marsh *et al*. (1994) to illustrate the 1988–92 UK drought and allows a direct comparison with their figure 18. SPIs 12 and 24 capture all the multi-annual droughts identified by Marsh *et al*. (1994), along with additional information about the intervening wet spells. SPIs 3 and 6 are seen to exhibit higher frequency variability. The correlations between the PDSI trace and SPI3, 6, 12, and 24 are 0.69, 0.81, 0.79, and 0.58 respectively, indicating closest agreement with SPI6 to SPI12.

3.3.2. Trends in drought/wetness. Figure 6 shows time series for the proportion of Europe experiencing moderate drought conditions as defined by the SPI3, SPI12, and PDSI ($SPI_n \leqslant -1$, $PDSI \leqslant -2$) indices. Again, a close correspondence is seen between SPI12 and the PDSI on annual and decadal scales, with $r = 0.73$.

Small negative trends are evident in both SPI time series, and a positive trend is observed in the PDSI series. Table IV shows the linear trends for 1901–99 for the proportion of Europe experiencing moderate drought/wetness ($|SPI| \geqslant 1$, $|PDSI| \geqslant 2$) and extreme drought/wetness ($|SPI| \geqslant 2$, $|PDSI| \geqslant 4$) conditions based on different indices. The SPI3 data in Table IV are also broken down by season, where $SPI3_{DJF}$ corresponds to the SPI3 February, $SPI3_{MAM}$ corresponds to the SPI3 May, etc. Inspection of Figure 6 indicates the presence of serial autocorrelation within the time series. This complicates the assessment of the significance trend. In the absence of autocorrelation an appropriate statistical test would be a *t*-test for the change in sample mean. Von Storch and Zwiers(1999) offer a variant of this test that allows for serial correlation. The relevant

Table IV. Linear trends 1901–99 in percentage of European area experiencing drought/wetness of different intensities for different indices and seasons in units of percentage change per year. Significant changes in the mean (at the 5% level using *t*-test adjusted for serial autocorrelation) are highlighted in bold

Condition	SPI3	$SPI3_{DJF}$	$SPI3_{MAM}$	$SPI3_{JJA}$	$SPI3_{SON}$	SPI12	PDSI
%Area extreme drought	0.003	0.026	0.012	0.015	−0.014	−0.006	0.017
%Area moderate drought	−0.005	0.009	0.019	0.026	−0.052	**−0.040**	0.068
%Area extremely wet	**0.022**	0.021	0.017	0.026	0.000	**0.030**	0.016
%Area moderately wet	**0.078**	**0.100**	0.066	0.053	0.021	**0.121**	0.017

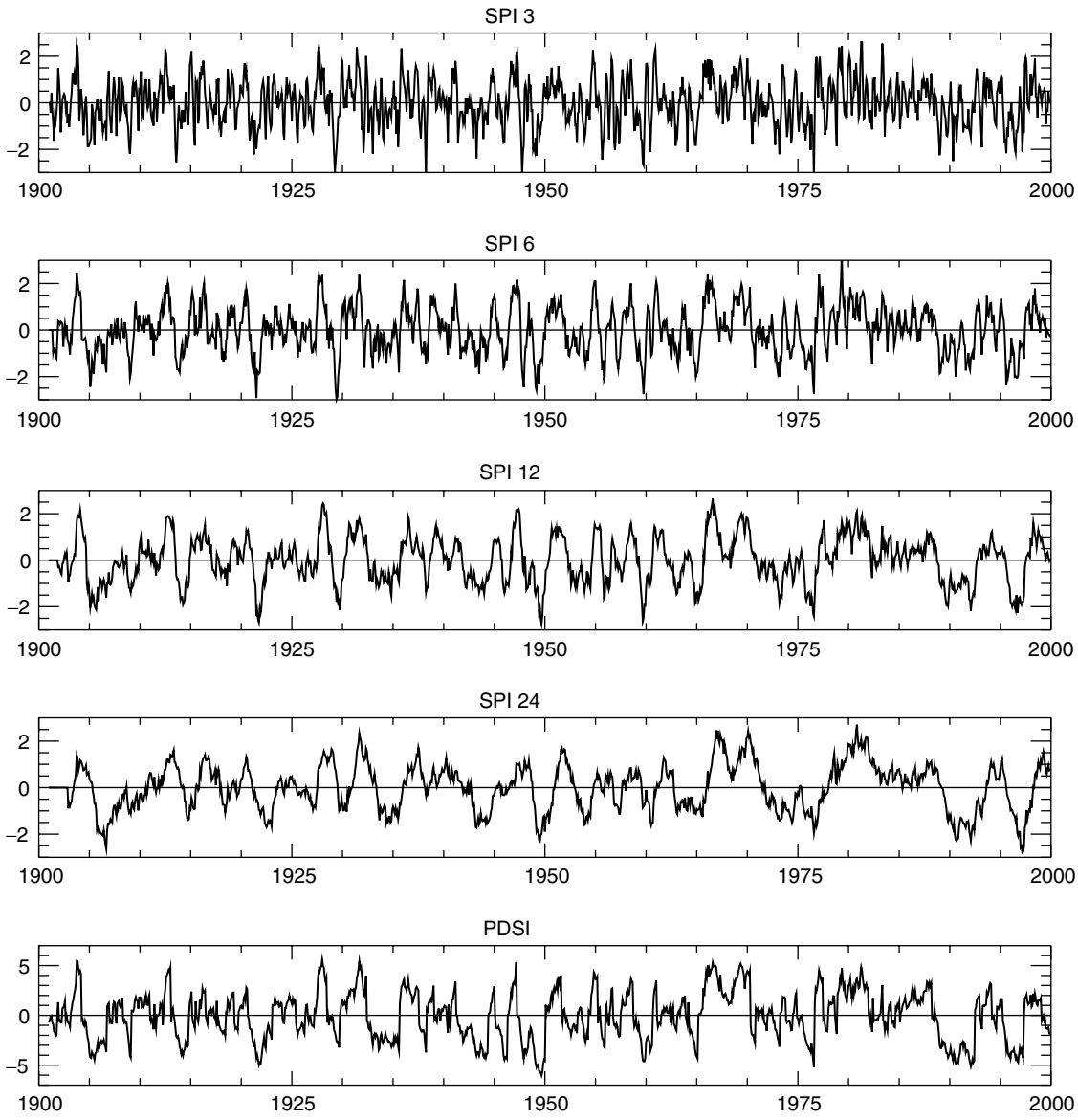

Figure 5. Drought severity index values representative of South Dalton, Yorkshire, UK, 1901–99. This site is selected for direct comparison with figure 18 of Marsh *et al*. 1994

statistic is

$$t' = \frac{\hat{\mu}_X - \hat{\mu}_Y}{\sqrt{\frac{s_X^2}{\hat{n}'_X} + \frac{s_Y^2}{\hat{n}'_Y}}} \tag{22}$$

where $\hat{n}'_X$ and $\hat{n}'_Y$ represent estimates of the effective sample size, defined as

$$\hat{n}'_X = \frac{n_X}{1 + \sum_{k=1}^{n_X - 1} \left(1 - \frac{k}{n_X}\right) \rho_X(k)} \tag{23}$$

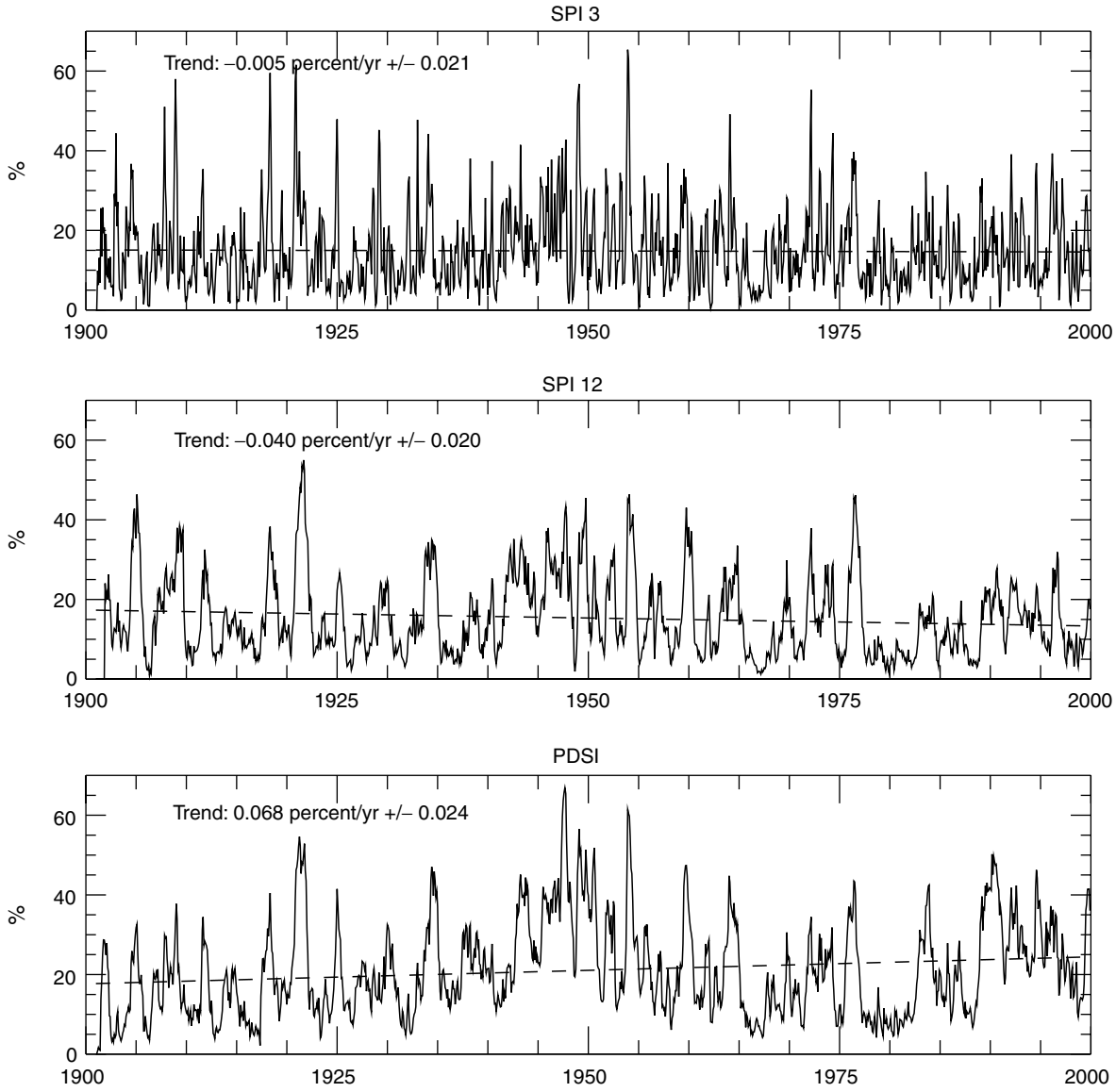

Figure 6. Proportion of Europe experiencing moderate drought conditions ($SPI_n \leqslant -1$, $PDSI \leqslant -2$). The dashed lines show the linear trend. Errors are ± 2 standard errors in the gradient

and $\rho_X(k)$ is the autocorrelation function

$$\rho_X(k) = \frac{1}{\sigma^2} \text{Cov } (\mathbf{X}_i,\ \mathbf{X}_{i+k}) \tag{24}$$

and where $\mathbf{X}$ is the autocorrelated time series. For large samples ($n_{X,Y} > 30$), t' follows the t-distribution. Linear trends that are significant at the 5% level after adjustment for serial autocorrelation are highlighted in bold in Table IV. The most significant trend is an increase in the percentage area experiencing moderately wet conditions at the 12 month time scale. A significant positive trend is also evident in SPI3. Analysis of the seasonal values of SPI3 reveals the wetness trend to be strongest in the winter/spring and weakest in summer/autumn.

For drought, we conclude that the proportion of Europe experiencing extreme and/or moderate drought conditions has changed insignificantly during the 20th century. Decadal trends in drought extent (Figure 6) are apparent, however, with greater pan-European drought incidence in the 1940s, early 1950s, and the 1990s, and lesser drought incidence in the 1910s, 1930s, and 1980s.

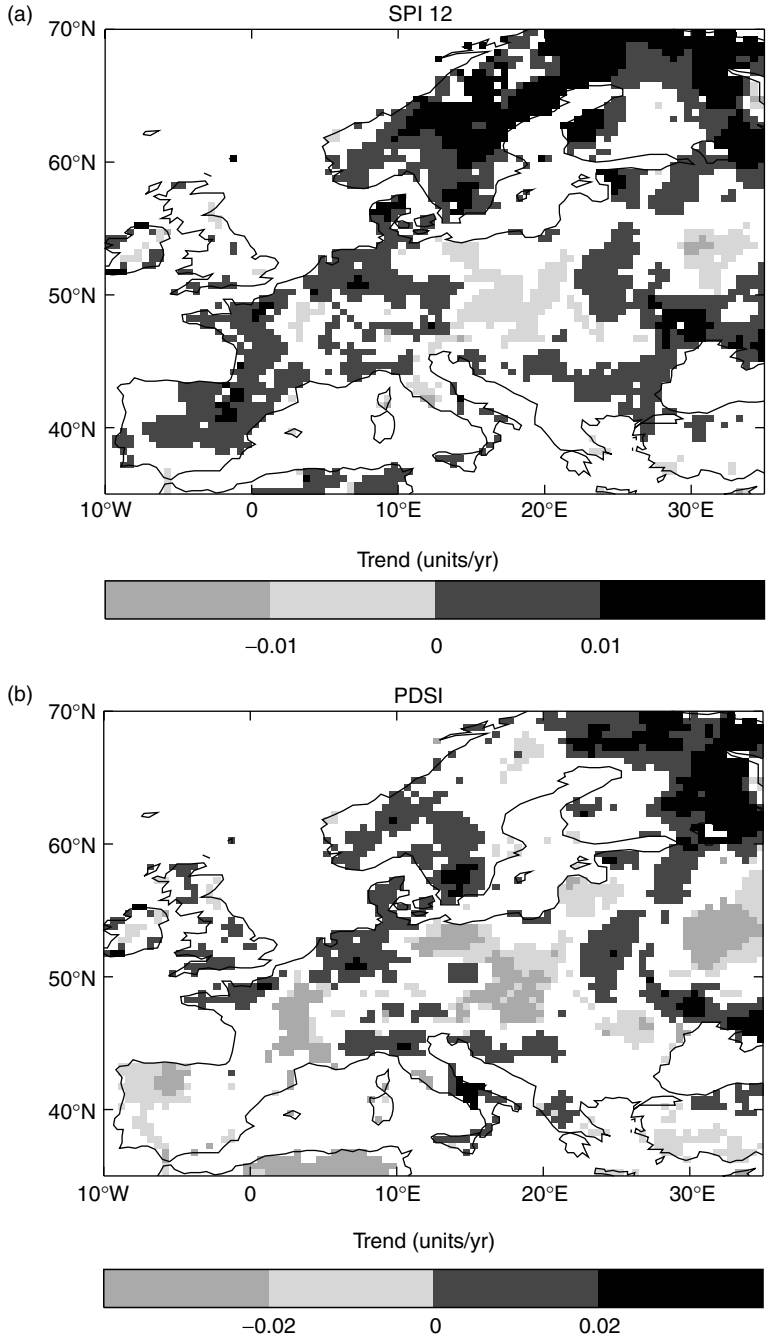

Figure 7. Map of significant linear trend 1901–99 in (a) SPI12 and (b) PDSI at the 10% level adjusted for autocorrelation

3.3.3. Spatial distribution of trend. Figure 7 illustrates the spatial distribution of linear trend in the values of (a) SPI12 and (b) the PDSI (filtered for significance at the 10% level after adjustment for temporal autocorrelation) for the period 1901–99. Spatial variation is evident across Europe. Significant positive trends are seen in both indices over large parts of Scandinavia, the Netherlands and the Ukraine. In contrast, areas of eastern Europe and western Russia have become drier during the 20th century. The pattern correlation between panels (a) and (b) is 0.82. Seasonal maps of SPI3 (not shown) for winter show similar trends and patterns to those observed in SPI12. Weaker, less distinct spatial differences in trend are seen in spring and autumn. Virtually no significant trends are detected during the summer.

3.3.4. Number of drought events. Figure 8 maps the number of extreme drought events ($SPI_n \leqslant -2$, $PDSI \leqslant -4$) by grid cell across Europe for 1901–99 computed from (a) SPI12 and (b) PDSI. Individual events are defined by zero crossings that bound the exceedance. The figure shows that the mean number of events is similar for both indices, but that the number of extreme droughts computed from the PDSI is more variable, i.e. the PDSI shows a greater range of values. Extreme droughts classified by the PDSI occur with a greater frequency over central and eastern Europe, and with a lower frequency along much of the northwestern seaboard, the Mediterranean seaboard, and the Alps. The spatial distribution of extreme drought frequencies for SPI12 is more homogeneous. Similarities do exist between Figure 8(a) and (b), for example over Italy and the Alps, but the overall agreement is poor, with a pattern correlation coefficient of just 0.25.

Table V lists the average number of exceedances by grid cell for extreme ($|SPI_n| \geqslant 2$, $|PDSI| \geqslant 4$) and moderate ($|SPI_n| \geqslant 1$, $|PDSI| \geqslant 2$) drought/wetness events for the period 1901–99. The data are further divided into two splits: 1901–50 and 1951–99. The mean number by grid cell of extreme and moderate European drought events, on a time scale of 12 months, is 6 ± 2 and 23 ± 3 events respectively during the 20th century. The mean number of droughts in each 50 year split is almost identical. In contrast, the mean number of extreme and moderate wet events have tended to increase from 1901–50 to 1951–99 (Table V).

3.3.5. Mean duration of droughts. A similar mapping, this time of the mean duration of extreme droughts, is shown in Figure 9. Structure is again visible within the plots, but this time there is more agreement between the PDSI and SPI12 classifications ($r = 0.45$). The longest mean extreme drought durations are found in Italy, northwest France, Finland, and northwest Russia. The clustering in these regions reflects spatial autocorrelation between neighbouring grid cells. Comparing Figure 9 with Figure 8 shows a tendency (in both the SPI12 and PDSI classifications) for regions of higher (lower) mean extreme drought duration to correspond to regions of lower (higher) mean drought number. Thus, where extreme droughts are more common their duration tends to be shorter, and *vice versa*.

Table V. Mean number of extreme ($|SPI_n| \geqslant 2$, $|PDSI| \geqslant 4$) and moderate ($|SPI_n| \geqslant 1$, $|PDSI| \geqslant 2$) drought/wet events across Europe for the periods 1901–99, 1901–50, and 1951–99. The duration of an event is defined as the time between the zero crossings that bound the event. Standard deviations are given in parentheses

Condition		SPI3	SPI6	SPI9	SPI12	SPI18	SPI24	PDSI
Extreme drought	1901–99	20(4)	12(3)	9(2)	6(2)	5(2)	3(1)	8(3)
	1901–50	10(4)	6(2)	5(2)	3(2)	3(1)	2(1)	4(2)
	1951–99	10(3)	6(2)	4(2)	3(2)	2(1)	1(1)	4(2)
Moderate drought	1901–99	68(6)	41(4)	30(4)	23(3)	16(3)	12(3)	26(4)
	1901–50	34(5)	21(3)	15(3)	12(2)	9(2)	7(2)	12(3)
	1951–99	34(5)	20(4)	14(3)	11(3)	8(2)	6(2)	14(3)
Extremely wet	1901–99	15(3)	10(2)	7(2)	6(2)	4(1)	4(1)	9(2)
	1901–50	6(3)	4(2)	3(2)	2(1)	2(1)	1(1)	4(2)
	1951–99	9(3)	6(2)	5(2)	4(1)	3(1)	2(1)	5(2)
Moderately wet	1901–99	65(6)	39(4)	28(4)	21(3)	15(3)	12(2)	28(4)
	1901–50	30(5)	18(4)	12(3)	9(3)	7(2)	5(2)	13(3)
	1951–99	35(4)	22(3)	16(3)	12(2)	9(2)	7(2)	15(3)

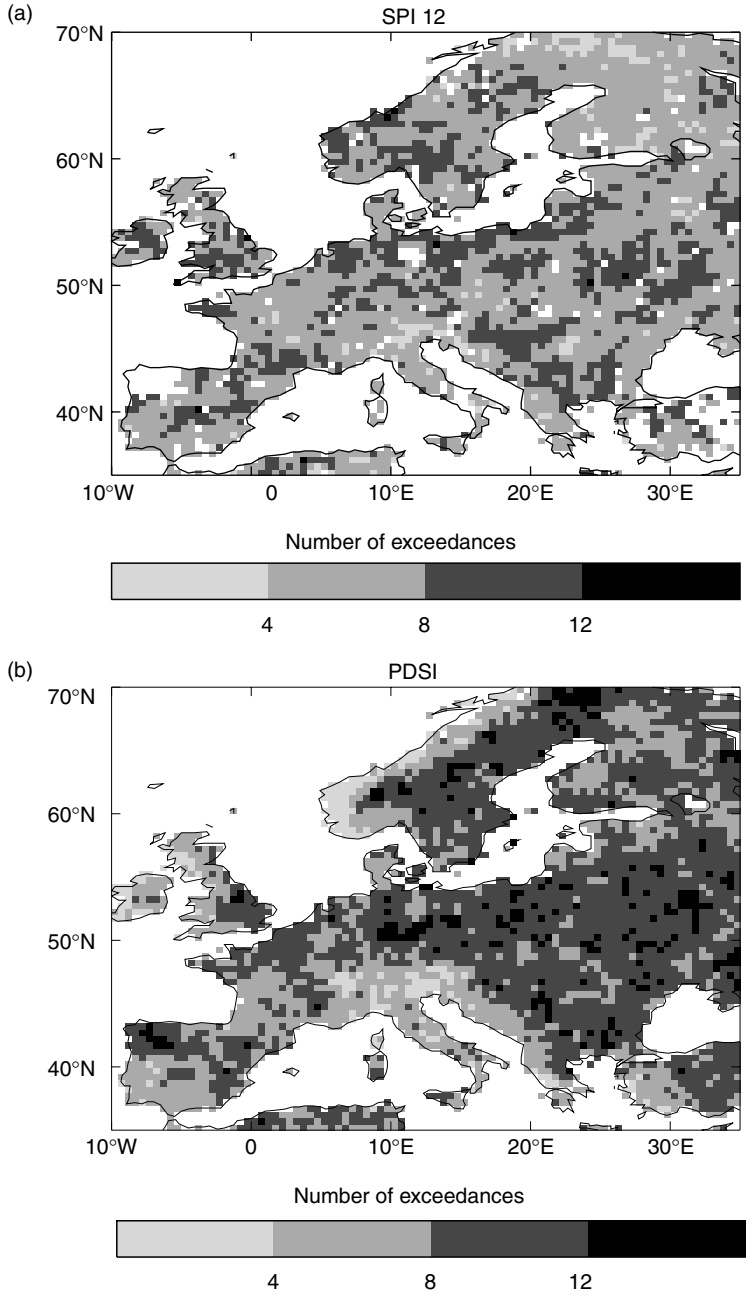

Figure 8. Number of extreme drought events ($SPI_n \leqslant -2$, PDSI $\leqslant -4$) by grid cell for Europe 1901–99 based on (a) SPI12 and (b) PDSI. Individual events are defined by the zero crossings that bound the exceedance

Table VI lists the mean duration by grid cell of extreme and moderate drought/wetness events across Europe. Durations are computed for the periods 1901–99, 1901–50, and 1951–99. Each grid cell is again weighted according to its area. The mean duration of extreme and moderate European drought events, on a time scale of 12 months, is 27 ± 8 months and 21 ± 3 months respectively. There is an indication that the mean duration has shortened during the 20th century. Comparison of the SPI and the PDSI index results

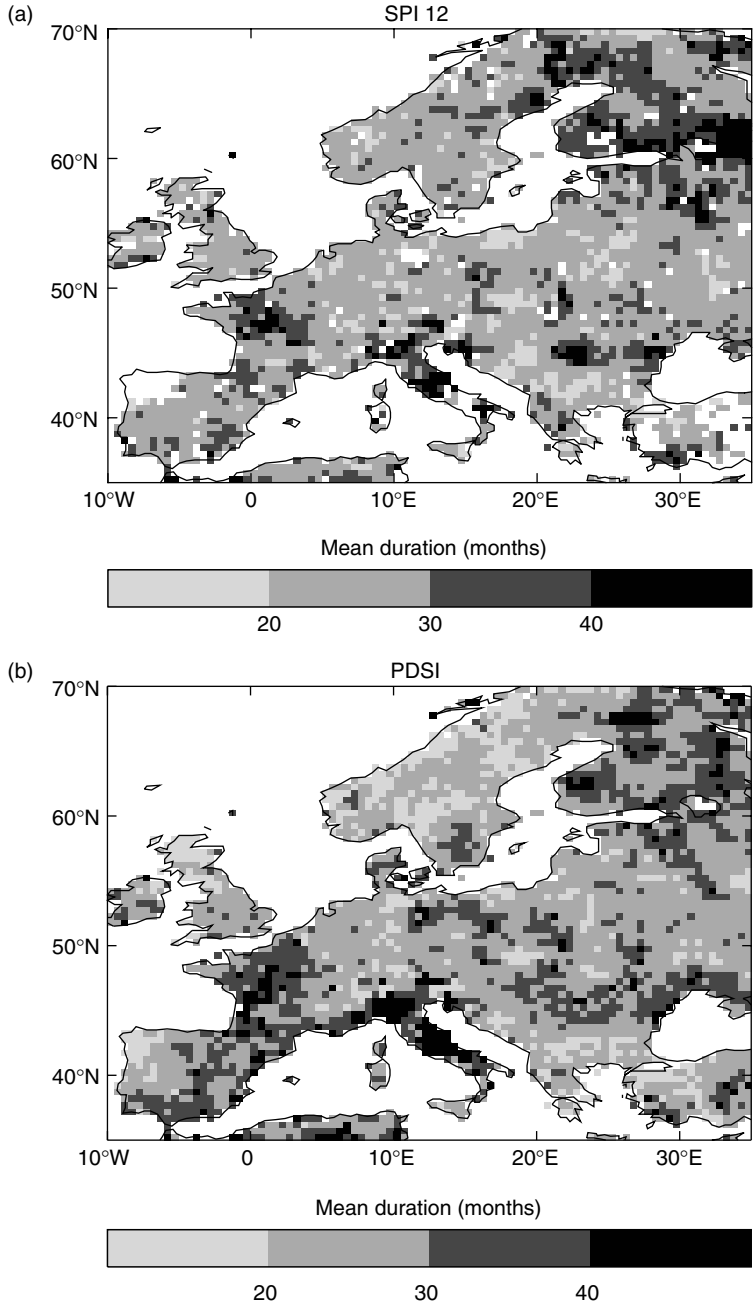

Figure 9. Mean duration of extreme drought events ($SPI_n \leqslant -2$, $PDSI \leqslant -4$) by grid cell for Europe 1901–99 for (a) SPI12 and (b) PDSI. Individual events are defined by the zero crossings that bound the exceedance

indicates best agreement with SPI12 for extreme drought durations and SPI9 for moderate drought durations. SPI3 drought durations are least variable, and last typically 6 to 8 months. The mean wetness durations in Table VI suggest a lengthening has occurred during the 20th century.

The mean durations computed for the splits in Table VI are systematically lower than those calculated from the full record. This is an artefact of the splitting process, since single events in the full record that

Table VI. Mean duration of extreme ($|SPI_n| \geqslant 2$, $|PDSI| \geqslant 4$) and moderate ($|SPI_n| \geqslant 1$, $|PDSI| \geqslant 2$) drought/wet events across Europe for the periods 1901–99, 1901–50, and 1951–99. The duration of an event is defined as the time between the zero crossings that bound the event. Standard deviations are given in parentheses

Condition		SPI3	SPI6	SPI9	SPI12	SPI18	SPI24	PDSI
Extreme drought	1901–99	8(1)	14(2)	20(4)	27(8)	40(15)	55(26)	28(8)
	1901–50	8(2)	15(4)	21(7)	28(11)	39(20)	51(34)	29(14)
	1951–99	7(2)	13(3)	18(6)	23(10)	30(17)	36(26)	24(10)
Moderate drought	1901–99	7(1)	11(1)	16(2)	21(3)	29(5)	39(9)	17(3)
	1901–50	7(1)	12(2)	17(3)	22(5)	31(8)	42(15)	19(5)
	1951–99	6(1)	10(2)	15(3)	19(4)	26(8)	33(11)	16(4)
Extremely wet	1901–99	8(1)	14(3)	21(4)	28(6)	38(11)	50(17)	25(7)
	1901–50	8(2)	14(5)	19(8)	23(12)	29(19)	34(26)	27(12)
	1951–99	8(2)	14(4)	20(6)	27(10)	37(16)	48(25)	23(9)
Moderately wet	1901–99	7(1)	12(1)	16(2)	21(3)	29(5)	38(8)	16(3)
	1901–50	7(1)	11(2)	16(3)	20(4)	28(7)	35(11)	17(5)
	1951–99	8(1)	12(2)	17(3)	22(5)	30(8)	39(11)	15(5)

extend through 1950–51 will be counted separately as two short events in the splits. The bias becomes more apparent when considering longer period events and extremes.

3.3.6. Maximum duration of droughts. Maps of the duration of the longest extreme drought for the period 1901–99 for a given grid cell (not shown) bear a close resemblance to those shown in Figure 9. This implies that the mean durations may be dominated by a few particularly long events.

Table VII lists the maximum duration by grid cell of extreme and moderate drought/wetness events across Europe. Durations are shown for 1901–99, 1901–50, and 1951–99. The mean maximum duration of extreme and moderate droughts, on a time scale of 12 months, is 48 ± 17 months and 56 ± 18 months respectively. Other findings parallel those for the mean duration of drought/wetness events (Section 3.3.5).

Table VII. Maximum duration of extreme ($|SPI_n| \geqslant 2$, $|PDSI| \geqslant 4$) and moderate ($|SPI_n| \geqslant 1$, $|PDSI| \geqslant 2$) drought/wet events across Europe for the periods 1901–99, 1901–50, and 1951–99. The duration of an event is defined as the time between the zero crossings that bound the event. Standard deviations are given in parentheses

Condition		SPI3	SPI6	SPI9	SPI12	SPI18	SPI24	PDSI
Extreme drought	1901–99	20(6)	30(10)	39(13)	48(17)	63(26)	79(37)	57(23)
	1901–50	18(7)	26(11)	34(15)	41(19)	52(30)	64(43)	47(25)
	1951–99	15(5)	22(8)	27(12)	32(16)	38(23)	42(31)	40(19)
Moderate drought	1901–99	27(9)	36(11)	46(14)	56(18)	73(26)	91(36)	59(22)
	1901–50	24(9)	33(11)	42(15)	50(18)	65(26)	80(39)	51(23)
	1951–99	21(7)	28(9)	34(11)	40(14)	50(20)	61(24)	44(17)
Extremely wet	1901–99	19(6)	28(8)	36(12)	46(16)	60(23)	72(29)	55(20)
	1901–50	14(5)	20(9)	25(12)	28(16)	34(23)	38(31)	44(30)
	1951–99	17(6)	25(9)	32(13)	40(18)	52(25)	63(34)	42(19)
Moderately wet	1901–99	30(10)	37(11)	46(14)	56(17)	71(23)	86(29)	57(19)
	1901–50	22(8)	28(9)	34(12)	40(14)	49(20)	59(25)	48(21)
	1951–99	26(10)	33(12)	41(15)	50(18)	64(24)	78(31)	44(17)

4. DISCUSSION

The gamma distribution provided the best fit of the models tested for describing monthly precipitation across Europe. The improvement in fit achieved by the gamma distribution over the normal is greatest for arid regions at short time scales. None of the distributions tested could adequately model precipitation over eastern Turkey or northwest Spain. This was true for all months and for all time scales. An improved fit for these regions could be achieved using a theoretical model with a narrow peak and long tails, such as the Cauchy distribution. However, it is unlikely that such a model would perform well outside of these regions. Given the relatively small fraction of the data that are invalid (6–15% of the study area), it seemed reasonable to simply exclude the invalid data from the rest of the analysis. Future work may lead to a multi-model scheme whereby precipitation data are standardized through transformation of the theoretical distribution that provides the best fit.

Trends in drought/wetness, though small for Europe as a whole, are significant over several European regions. Upward trends in wetness are largest over northeast Europe during winter and spring. These results agree with the IPCC report findings on the regional impacts of climate change (Watson *et al*., 1997) which show a precipitation increase over the region from the Alps to northern Scandinavia since 1900. The drying tendencies found in central eastern Europe and western Russia since 1900 are also in accord with the IPCC findings.

Extreme droughts, as classified by the PDSI, occur with greater frequency over continental eastern Europe. Conversely, droughts are rarer along the northwest European seaboard, the Mediterranean seaboard, and the Alps. The SPI is found to be homogeneous with respect to the spatial distribution of extreme drought events. Hayes *et al*. (1999) cite the inability of the SPI to identify those regions that are more drought prone as a potential disadvantage. However, standardization in space and time is precisely what is required from a standard classification scheme where the frequency of a given event should be independent of location. Thus, the SPI should be viewed as superior to the PDSI for classifying droughts on a standard consistent scale. Apart from the spatial distribution of drought incidence, the SPI12 index yields results nearly identical to those obtained using the PDSI. This agrees with Oladipio (1985), who, using data for Nebraska, showed that indices based solely on precipitation can perform well when compared with more complex hydrological indices such as the PDSI. The SPI has the additional advantage of a variable time scale, which can benefit investigations of the temporal evolution of particular events (e.g. the US 1996 drought (Hayes *et al*., 1999)).

5. CONCLUSIONS

We have presented a new high spatial resolution, multi-temporal climatology for the incidence of 20th century European drought. The climatology is based on monthly SPIs calculated on a 0.5 °grid across the whole of Europe for the period 1901–99.

The gamma distribution has been found to provide the best model for describing monthly precipitation over most of Europe. Notable exceptions occur in northwest Spain and eastern Turkey, where the equiprobability transform of the data into the standardized normal distribution fails and the resultant SPI values are invalid. Given the small fraction of the data that are invalid (6–15% of the study area), no attempt has been made to standardize the data by other means. Invalid data have simply been excluded from the analysis.

We have compared characteristics of the SPI computed over time scales of 3 to 24 months with the PDSI. In general, SPI12 exhibits a close correspondence to the PDSI. This agrees with the findings of previous studies, e.g. Guttman (1998) for the USA, and Bussay *et al*. (1998) for Hungary. It is clear that much of the variability seen in the PDSI results directly from precipitation.

Trends in SPI and PDSI values indicate that the proportion of Europe experiencing extreme and/or moderate drought conditions has changed insignificantly during the 20th century. Spatially, changes in the mean value of both indices are found to be variable, with a significant shift towards wetter conditions observed over northeast Europe. Drying tendencies are observed over central eastern Europe and western Russia. Trends are strongest in winter/spring and weakest in the summer/autumn.

Analysis of extreme drought events shows the SPI provides a better spatial standardization than the PDSI. Extreme droughts, as classified by the PDSI, occur with a greater frequency within the interior of continental Europe. Conversely, they are less common along the northwest European seaboard, the Mediterranean seaboard, and the Alps. Extreme droughts, as classified by both the PDSI and SPI12, are found to persist on average for 2–3 years, with the most extreme droughts lasting in excess of 5 years. Regionally, the longest droughts are found in Italy, northwest France, and northwest Russia, with typical durations of 40 months.

In summary, this paper has shown the SPI is a simple and effective tool for the study of European drought. A new high-resolution climatology of SPI values has been created and validated. We hope this climatology will provide a useful resource for assessing European drought vulnerability on different spatial and temporal scales, and for initiating investigations into the seasonal predictability of European drought incidence.

ACKNOWLEDGEMENTS

Benjamin Lloyd-Hughes is supported by a Research Studentship from the UK Natural Environment Research Council. He gratefully thanks St. Paul Re. for industrial CASE sponsorship. We thank Richard Heim at NOAA for supplying the code used to calculate the PDSI values. The CRU 0.5° lat/lon gridded monthly climate data were supplied by the Climate Impacts LINK Project (UK Department of the Environment Contract EPG 1/1/16) on behalf of the Climatic Research Unit, University of East Anglia, UK.

REFERENCES

Abramowitz M, Stegun A (eds). 1965. *Handbook of Mathematical Formulas, Graphs, and Mathematical Tables*. Dover Publications, Inc.: New York.

Alley WM. 1984. The Palmer drought severity index: limitations and assumptions. *Journal of Climate and Applied Meteorology* **23**: 1100–1109.

Briffa KR, Jones PD, Hulme M. 1994. Summer moisture variability across Europe, 1892–1991: an analysis based on the Palmer drought severity index. *International Journal of Climatology* **14**: 475–506.

Bussay AM, Szinell C, Hayes M, Svoboda M. 1998. Monitoring drought in Hungary using the standardized precipitation index. Annales Geophysicae, Supplement 11 to Vol 16, the Abstract Book of 23rd EGS General Assembly, C450. April 1998, Nice; France.

Bussay A, Szinell C, Szentimery T. 1999. *Investigation and Measurements of Droughts in Hungary*. Hungarian Meteorological Service: Budapest.

Demuth S, Stahl K, (eds). 2001. Assessment of regional impact of droughts in Europe. Final report to the European Union ENV-CT97-00553. Institute of Hydrology, University of Freiburg: Freiburg, Germany.

Edwards DC, McKee TB. 1997. Characteristics of 20th century drought in the United States at multiple timescales. Colorado State University: Fort Collins. Climatology Report No. 97-2.

Estrela MJ, Penarrocha D, Millán M. 2000. Multi-annual drought episodes in the Mediterranean (Valencia region) from 1950–1996. A spatio-temporal analysis. *International Journal of Climatology* **20**: 1599–1618.

European Environment Agency. 2001. Sustainable water use in Europe, Part 3: extreme hydrological events: floods and droughts. Environmental Issue Report No. 21.

FAO. 1996. *The Digitized Soil Map of the World Including Derived Soil Properties* (CD-ROM). Food and Agriculture Organization: Rome.

Gibb O, Penman HL, Pereier HC, Ratcliffe RAS. 1978. *Scientific Aspects of the 1975–76 Drought in England and Wales*. The Royal Society: London.

Guttman NB. 1998. Comparing the Palmer drought severity index and the standardised precipitation index. *Journal of the American Water Resources Association* **34**: 113–121.

Hayes MJ, Svoboda MD, Wilhite DA, Vanyarkho OV. 1999. Monitoring the 1996 drought using the standardized precipitation index. *Bulletin of the American Meteorological Society* **80**: 429–438.

Karl TR. 1983. Some spatial characteristics of drought duration in the United States. *Journal of Climate and Applied Meteorology* **22**: 1356–1366.

Kilsby CG (ed.). 2001. Water resources: influence of climate change in Europe ENV4-CT97-0452. Water Resource Systems Research Laboratory, University of Newcastle: Newcastle-Upon-Tyne, UK.

Lana X, Serra C, Burgueño A. 2001. Patterns of monthly rainfall shortage and excess in terms of the standardized precipitation index. *International Journal of Climatology* **21**: 1669–1691.

Marsh TJ, Lees ML. 1985. *The 1984 Drought*. Institute of Hydrology: Wallingford, UK.

Marsh TJ, Monkhouse RA, Arnell NW, Lees ML, Reynard NS. 1994. *The 1988–92 Drought*. Institute of Hydrology: Wallingford, UK.

McKee TB, Doesken NJ, Kliest J. 1993. The relationship of drought frequency and duration to time scales. In *Proceedings of the 8th Conference on Applied Climatology, 17–22 January, Anaheim, CA*. American Meteorological Society: Boston, MA; 179–184.

New M, Hulme M, Jones P. 2000. Representing twentieth-century space–time climate variability, part II: development of 1901–96 monthly grids of terrestrial surface climate. *Journal of Climate* **13**: 2217–2238.

Nigam S, Barlow M, Berbery EH. 1999. Analysis links Pacific decadal variability to drought and streamflow in United States. *EOS Transactions of the American Geophysical Union* **80**: 621–625.

Oladipio EO. 1985. A comparative performance analysis of three meteorological drought indices. *International Journal of Climatology* **5**: 655–664.
Palmer WC. 1965. *Meteorological drought*. Research Paper No. 45. US Weather Bureau: Washington, DC.
Phillips ID, McGregor GR. 1998. The utility of a drought index for assessing the drought hazard in Devon and Cornwall, South West England. *Meteorological Applications* **5**: 359–372.
Press WH, Flannery BP, Teukolsky SA, Vetterling WT. 1986. *Numerical Recipes*. Cambridge University Press: Cambridge.
Reynolds CA, Jackson TJ, Rawls WJ. 1999. Estimating available water content by linking the FAO soil map of the world with global soil profile databases and pseudo-transfer functions. Proceedings of the American Geophysical Union: Spring Conference, Boston, MA.
Soulé PT. 1992. Spatial patterns of drought frequency and duration in the contiguous USA based on multiple drought event definitions. *International Journal of Climatology* **12**: 11–24.
Szalai S, Szinell C. 2000. Comparison of two drought indices for drought monitoring in Hungary — a case study. In *Drought and Drought Mitigation in Europe*, Vogt JV, Somma F (eds). Kluwer: Dordrecht; 161–166.
Thom HCS. 1958. A note on the gamma distribution. *Monthly Weather Review* **86**: 117–122.
Von Storch H, Zwiers W. 1999. *Statistical Analysis in Climate Research*. Cambridge University Press: Cambridge.
Watson RT, Zinyowera MC, Moss RH (eds). 1997. *The Regional Impacts of Climate Change: An Assessment of Vulnerability*. Cambridge University Press: Cambridge.
Wilhite DA, Glantz MH. 1985. Understanding the drought phenomenon: the role of definitions. *Water International* **10**: 111–120.
Wilks DS. 1995. *Statistical Methods in the Atmospheric Sciences*. Academic Press: London.

